Supplementary Information

Spatial characterization of redox processes and speciation of Ru(III) anticancer complexes by ^{19}F magnetic resonance imaging

Gregory A. MacNeil,[a] Stephanie W. Chang,[a] Kathleen E. Prosser,[a] Eric Ye,[a] Devon Heroux,[b] Andrew R. Lewis[a,c] Marcel Bally,[b] and Charles J. Walsby[a,*]

a) Department of Chemistry, Simon Fraser University, 8888 University Dr., Burnaby, BC, V5A 1S6, Canada.

b) BC Cancer Research Institute, 675 West 10th Ave., Vancouver, BC, V5Z 1L3, Canada.

c) Callaghan Innovation, 69 Gracefield Rd, Lower Hutt, 5010, New Zealand.

* Corresponding author

Table of Contents

S1. Synthesis and Reduction of Complexes

S1.1 Synthesis

$Na[RuCl_4(CF_3Im)_2]$ (**Ru(III)(ImCF$_3$)$_2$**) was synthesized as previously reported.[1] For imaging experiments the complex was reduced to **Ru(II)(ImCF$_3$)$_2$** using 1.5 equivalents of sodium dithionite (NaDT) (Sigma-Aldrich) in phosphate buffered saline (PBS: NaCl (150 mM), KH_2PO_4 and K_2HPO_4 (10 mM) corrected to pH 7.4) that was previously purged with N_2.

S1.2 Choice of Reducing Agent

Three reducing agents, sodium ascorbate (NaAsc), reduced *L*-glutathione (GSH) (Sigma-Aldrich), and NaDT, were tested for reduction of a 4 mM solution of **Ru(III)(ImCF$_3$)$_2$** to **Ru(II)(ImCF$_3$)$_2$**. These experiments used 1.5 equivalents of the reducing agents in deoxygenated PBS at room temperature. Reduction processes were monitored by ^{19}F NMR, and signals consistent with reduction of **Ru(III)(ImCF$_3$)$_2$** where detected in each case (**Figure S1.1**). Sodium dithionite gave a clean reduction of **Ru(III)(ImCF$_3$)$_2$** to **Ru(II)(ImCF$_3$)$_2$** (**Figure S1.1c**), which remained as the majority species over 18 h at room temperature. A second signal from a species with a similar chemical shift was observed, corresponding to chloride ligand exchange leading to a monoaqua Ru(II) species, likely [*trans*-Ru(II)$Cl_3(H_2O)$(5-(CF_3)-1*H*-imidazole)$_2$]$^-$. A minor signal at lower chemical shift was also detected after longer incubation, and was identified as a small contribution from free ligand. Reduction with *L*-glutathione resulted in a very similar spectrum after 1 hour to that with sodium dithionite (**Figure S1.1b**), demonstrating that the same reduced Ru species were generated. Reaction with ascorbate also showed signals after 1 h that were similar to those following reduction with sodium dithionite, but with some additional peaks, notably at −52.5 ppm and at higher chemical shifts, and with a weaker signal overall (**Figure S1.1a**).

S2. Magnetic Resonance Methods

Magnetic resonance experiments were performed on a Bruker AVANCE III 400WB spectrometer. A Bruker MicWB40 Probe with interchangeable RF coils was used and tuned to either ^{1}H (400 MHz) or ^{19}F (376 MHz). A water-cooled Bruker Micro2.5 MicWB40 gradient coil system was mounted inside the room temperature shim set. A 20 mm internal diameter dual-channel ^{1}H/^{19}F birdcage coil was mounted on the MicWB40 Probe.

^{19}F T_1 measurements were conducted without ^{1}H decoupling. Typical parameters were as follows: sweep width, 60 ppm; transmitter offset 1.50 ppm; pulse angle, 90°; pulse length 28.3 μs; acquisition time 0.33 s; recycle delay 0.50 s; number of dummy scans, 4; number of data points 32,768; number of scans, 4; pulse sequence, inversion recovery; relaxation delays, 0.1, 0.2, 0.3, 0.4, 0.5, 0.75, 1, 1.5, 2, and 4 seconds. Spectra were processed in TOPSPIN v2.1 using 2 Hz exponential apodization and zero-filling to 32,768 points before the Fourier transform. T_1 values (**Table S2.1**) were determined using the T_1 analysis routine in TopSpin. Experiments were conducted at 25 or 37 °C using a Bruker BVT 3000 temperature controller, which monitored and maintained the temperature of the heated air stream passed over the sample vial.

Data from ^{1}H/^{19}F CHESS and CSI experiments were processed using the Bruker software ParaVision v5.1 and the included CSI visualization tool. Fat (tissue) and motion suppression (heating effect) was activated for the ^{1}H CHESS experiments.[2]

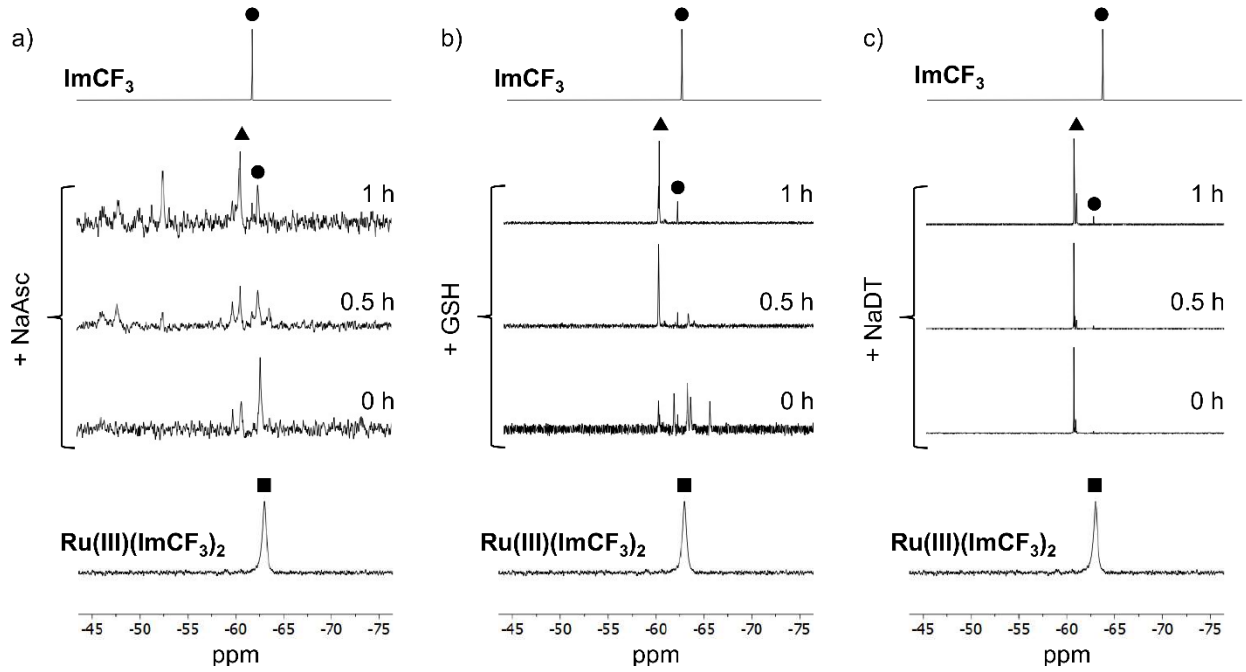

Figure S1.1. ^{19}F NMR of **Ru(III)(ImCF$_3$)$_2$** in N_2 purged PBS at 0, 0.5 and 1 h at room temperature after the addition of 1.5 equivalents of a) sodium ascorbate, b) reduced *L*-glutathione, and c) sodium dithionite. The bottom spectrum in each panel is unreduced **Ru(III)(ImCF$_3$)$_2$** (■) in PBS and the top is the **ImCF$_3$** ligand (●) in PBS. After 1 h incubation, reduction generates **Ru(II)(ImCF$_3$)$_2$** and the ligand-exchange product [*trans*-Ru(II)Cl$_3$(H$_2$O)(5-(CF$_3$)-1*H*-imidazole)$_2$]$^-$ (both signals indicated by ▲).

Table S2.1. ^{19}F T_1 and T_2 (ms) for **Ru(III)(ImCF$_3$)$_2$** and **Ru(II)(ImCF$_3$)$_2$** at 25 °C and 37 °C in PBS.

	PBS (25 ˚C)		PBS (37 ˚C)	
	T_1	T_2	T_1	T_2
Ru(III)	70.0	9.23	83.0	25.4
Ru(II)	250	207	210	135

S2.1. Pulse Sequences

The rapid acquisition with relaxation enhancement (RARE) pulse sequence was used for CHESS. This sequence utilizes a single 90° excitation pulse followed by a specified number of 180° refocusing pulses. The number of refocusing pulses (RARE factor) allows for several echoes to be acquired during a single pulse sequence.[3] The resulting refocused spins are spatially oriented by applying phase- or frequency-encoding over a sample using an external field gradient.[4] These gradients are applied to each refocused echo, which reduces acquisition times compared to traditional spin-echo sequences. The reduction in acquisition time is defined by the RARE factor (e.g., a RARE factor of 4 is 4× faster). For ^{19}F CSI experiments a basic pulse-acquire sequence was used as this allowed for the use of short TE (6.5 ms) given the fast T_2 relaxation time of the complex, and the shorter overall acquisition time.

S2.2. Typical ^{1}H CHESS Protocol

A 10 × 75 mm test tube containing the tissue sample elevated on four 4-mm dia. glass beads in a 4 mM solution of **Ru(III)(ImCF$_3$)$_2$** or **Ru(II)(ImCF$_3$)$_2$** in PBS was placed into a Styrofoam support in the 20 mm imaging coil to ensure it was centred in the RF coil. A sagittal ^{1}H CHESS image was collected with a field of view of 1.5 cm^2, 256 × 256 matrix size, and a slice thickness of 0.25 mm. A slice-selective 90° excitation pulse was used with: pulse length, 2.70 ms; bandwidth, 2000 Hz; attenuation, 20 dB; pulse shape, Bruker ParaVision5.1 – Hermite. A 180° refocusing pulse was used with: pulse length, 1.71 ms; bandwidth, 2000 Hz; attenuation, 10 dB; pulse shape, Bruker ParaVision5.1 – Hermite. The repetition time (TR) was set to 500 ms and the echo time (TE) was set to 8.5 ms. A RARE factor of 4 was used where 10 averages resulted in an acquisition time (TA) of 4 min.

S2.3 Typical ^{19}F CHESS Protocol

A ^{19}F CHESS image was collected on a 20 mm thick axial slice of a tube-in-tube (see S3.1) sample with a field of view of 2.0 cm^2 and a 64 × 64 voxel matrix. A slice-selective 90° excitation pulse was used with: pulse length, 1.00 ms; bandwidth, 5400.0 Hz; attenuation, 16.5 dB; pulse shape, Bruker ParaVision5.1 – Hermite. A 180° refocusing pulse was used with: pulse length, 0.34 ms; bandwidth, 10058.8 Hz; attenuation, 0.5 dB; pulse shape, Bruker ParaVision5.1 – Hermite. The relatively short T_1 times for **Ru(III)(ImCF$_3$)$_2$** and **Ru(II)(ImCF$_3$)$_2$** allowed for TR to be set to 300 ms. With a TE of 8.5 ms and a RARE factor of 4, 1000 averages resulted in an acquisition time of 1 h.

S2.4 Typical ^{19}F CSI Protocol

An 8 × 8 matrix of voxels was collected with a TR of 300 ms and TE of 8.5 ms, resulting in a TA of 6 min for 1024 scans and 23 averages. Axial slices were selected with thicknesses that varied depending on the sample. A slice-selective 90° excitation pulse was used with: pulse length, 0.50 ms; bandwidth, 12420.0 Hz; attenuation, 10.1 dB; pulse shape, Bruker ParaVision5.1 – sinc3. A weighted filter was used and the resulting matrix was upscaled to 16 × 16 with zero-filling [5]

S3. Sample Preparation

S3.1 Tube-in-tube Experiments: Ru(III)(ImCF$_3$)$_2$ and Ru(II)(ImCF$_3$)$_2$

Tube-in-tube experiments involved dissolving **Ru(III)(ImCF$_3$)$_2$** in PBS to give a final concentration of 4 mM and placing the solution into a 10 × 75 mm test tube. Sodium dithionite (6 mM) was added to a second 4 mM solution of **Ru(III)(ImCF$_3$)$_2$** in N_2 purged PBS to generate the reduced complex, **Ru(II)(ImCF$_3$)$_2$**. This solution was placed in a 4 mm dia. NMR tube and centred in the test tube containing the **Ru(III)(ImCF$_3$)$_2$** solution. The sample heights in each tube were approx. 25 mm and the tube-in-tube setup was then centred in the 20 mm imaging coil using Styrofoam shims.

S3.2 Beef Liver Experiments

Beef liver was purchased from Nesters Market, SFU and approximately 1 cm^3 piece were placed in 10 × 75 mm test tubes and elevated on four 4-mm dia. glass beads. A 4 mM solution of either

Ru(III)(ImCF$_3$)$_2$ or **Ru(II)(ImCF$_3$)$_2$** in PBS was injected into the liver via syringe. The test tube was then centred in the 20 mm imaging coil with Styrofoam.

S3.3 Tumor Growth, Excision, and Measurements

Mouse tissue was provided by BC Cancer Research Institute (Dr. Bally; PI), and the mice used were obtained via a University of British Columbia (UBC) approved animal care protocol (A18-0276). Studies conducted under this protocol meet Canadian Council of Animal Care guidelines and ongoing oversight of animals held under this protocol is managed through UBC's Animal Care Committee Post-approval monitoring team.

Severely immunodeficient NRG mice were injected subcutaneously with 1×10^7 MBA-MB-231 human breast adenocarcinoma cells (American Type Culture Collection, ATCC, Manassas, Virginia, USA). Tumor growth was measured 3 times per week with calipers and the tumor volume was calculated based on a formula of $V = (L \times W^2)/2$. When the volume exceeded 800 mm^3, the animal was sacrificed, and the tumor was excised and stored on ice.

The MDA-MB-231 tumor, which was approximately 0.7 cm in diameter, was placed in a 10 × 75 mm test tube and elevated on four 4 mm dia. glass beads. A 4 mM solution of either **Ru(III)(ImCF$_3$)$_2$** or **Ru(II)(ImCF$_3$)$_2$** in PBS was injected into the tumor via syringe, and the tumor was then placed in a test tube containing the same solution. The test tube was then centred in the 20 mm imaging coil with Styrofoam shims.

S3.4 Preparation of ^{19}F CSI Calibration Samples

Four samples of **Ru(III)(ImCF$_3$)$_2$** in PBS at 1, 2.5, 5, and 10 mM were prepared and 700 µL of each were placed in separate NMR tubes. These four NMR tubes were then placed inside a 16 × 150 mm test tube which was filled with PBS to match the sample heights in the NMR tubes. The final sample height was 35 mm. This setup was then placed in the 20 mm imaging coil and aligned with Styrofoam.

S4. Data Processing

S4.1 ^{19}F CHESS Data Processing

To remove noise due to voxels containing signal artefacts, and improve the overall image quality, a step-wise signal processing protocol was applied. The data resulting from the ^{19}F CHESS images of the tube-in-tube setup were processed in Matlab using the suggested methods and open source toolboxes created by Starke *et al*.[6] Briefly, image data were corrected for Rician noise bias using a lookup table for the RF coil with two receive elements used in these experiments.[7] The noise was then calculated as the standard deviation of the signal in a square region (10 × 10 voxels) in all four corners of the image, which contained no signal, and was corrected by a factor related to the two receive elements.[8] Subsequently, following the approach of Starke *et al*,[6] all voxels with an SNR less than 2.74 were set to zero SNR. Next, outlier voxels, lacking at least three signal-containing neighbours (8 connected neighbours by edges and corners) were set to zero SNR. The raw data image and resulting images from each processing step can be seen in **Figure S4.1**.

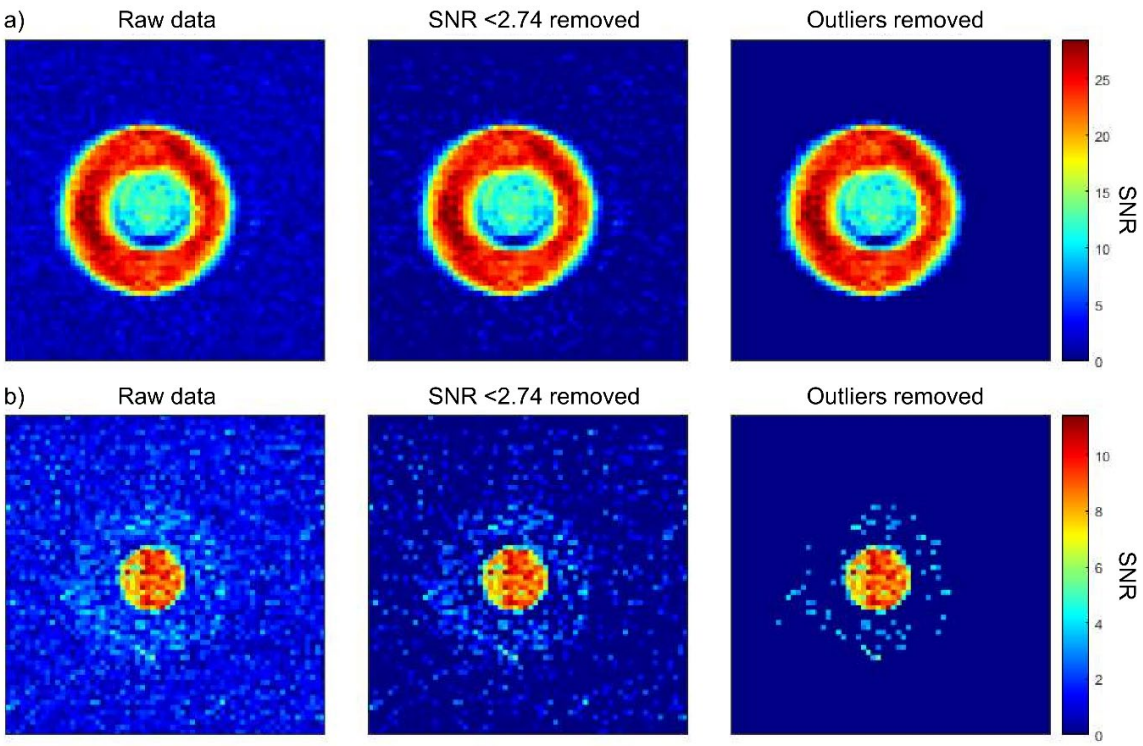

Figure S4.1 Raw and processed ^{19}F CHESS images of the tube-in-tube experiment plotted as the SNR in each voxel where: a) is the image collected with a TE of 8.5 ms and b) is the image collected with a TE of 42.5 ms following a single excitation pulse.

S4.2 ^{19}F CSI data processing

^{19}F CSI data was processed following similar methods described in S4.1 with slight variation. The signal in each voxel was corrected to the number of scans in each voxel as set by the weighted filter in ParaVision5.1. The noise was calculated from a region of each spectra containing no signal and averaged over all voxels.

S4.3 Calculation of the Number ^{19}F Atoms per Voxel

A custom program was written in Matlab to first generate a calibration curve relating the SNR over a region of interest (ROI) to the concentration of **Ru(III)(ImCF$_3$)$_2$** in PBS from the data generated from a ^{19}F CSI calibration experiment. The ROI was selected using a ^{1}H anatomical reference scan and applied to the ^{19}F CSI data. The ^{19}F CSI SNR data was then summed over the ROI. (**Figure S4.3**). The resulting data were fit to a linear function.

Next a ROI was selected using an anatomical ^{1}H CHESS image of the tumor and applied to the corresponding ^{19}F CSI matrix, as above. The summed SNR over the ROI was used in the linear fit equation to solve for concentration. The resulting concentration of the entire ROI was divided by the number of voxels in the ROI to give concentration per voxel, which was used to calculate the number of ^{19}F atoms per voxel in the tumor tissue. The error in the resulting value was calculated using the root mean square error (RMSE) of the fit and the standard deviation of the parameters of the linear equation generated by the 'polyfitn' function in Matlab.

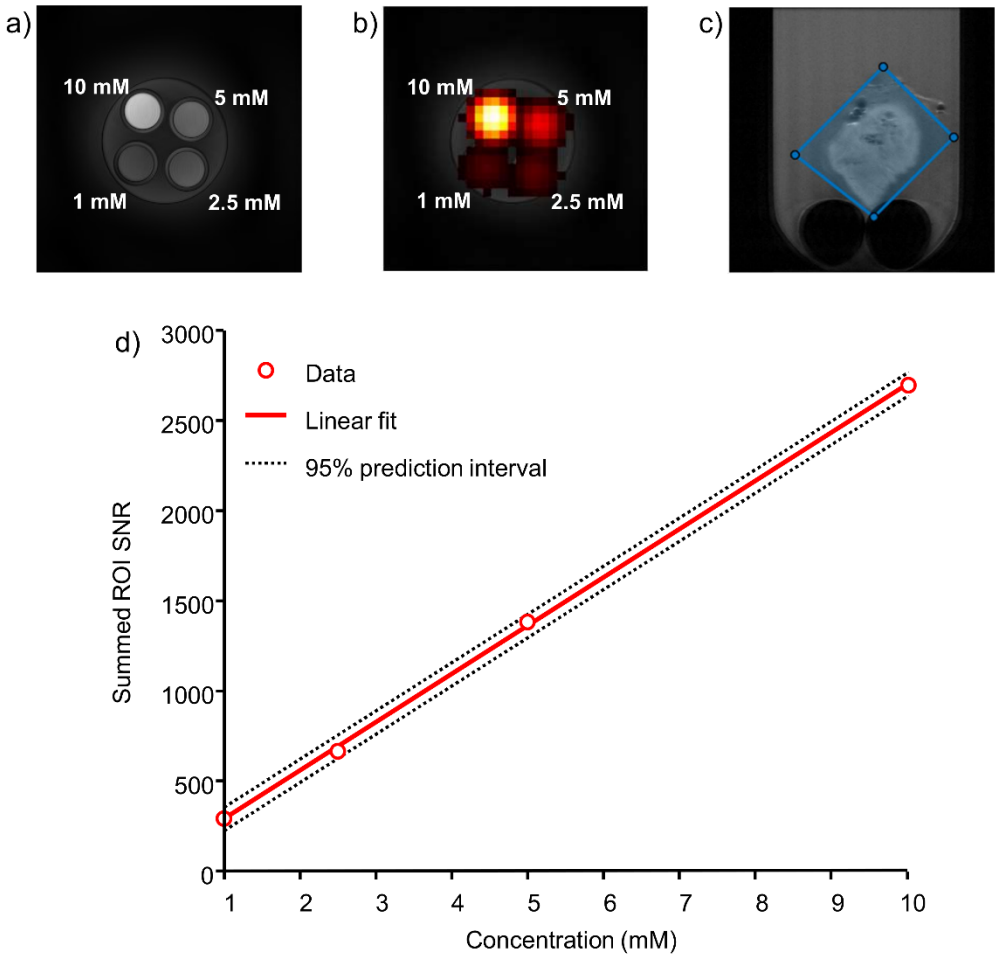

Figure S4.2 a) Anatomical ^{1}H CHESS image of the four calibration samples of **Ru(III)(ImCF$_3$)$_2$** in PBS used for the ROI selection. b) Overlay of ^{19}F CSI SNR onto the anatomical ^{1}H CHESS image. c) An example of the ROI selected from a ^{1}H CHESS image of tumor tissue used to calculate the number of ^{19}F atoms per voxel from a corresponding ^{19}F CSI experiment. d) Linear fit to summed ^{19}F CSI SNR over the ROI versus concentration from the calibration sample. Dashed lines represent the bounds of two standard deviations from the fit.

S5. ^{19}F CSI Data

S5.1 Varied TR in Beef Liver Tissue

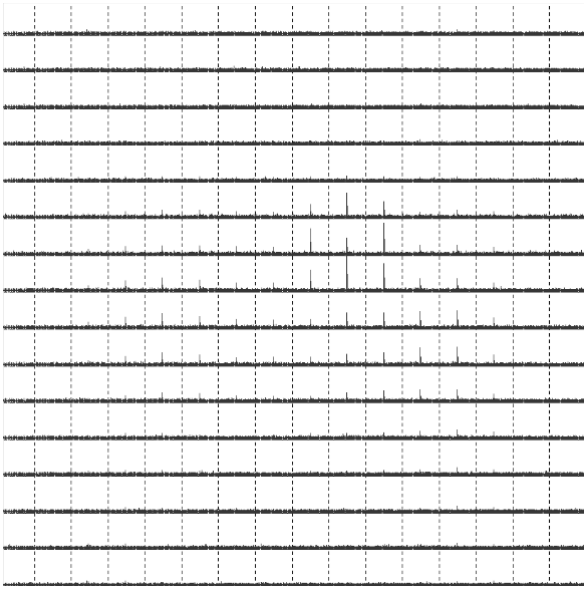

Figure S5.1 ^{19}F CSI matrix of a piece of beef liver following injection of a 4 mM PBS solution of **Ru(III)(ImCF$_3$)$_2$**. The tumour was then placed back in the same solution in a test-tube. The ^{19}F CSI parameters were as described in section S2.4 with TR 100 ms.

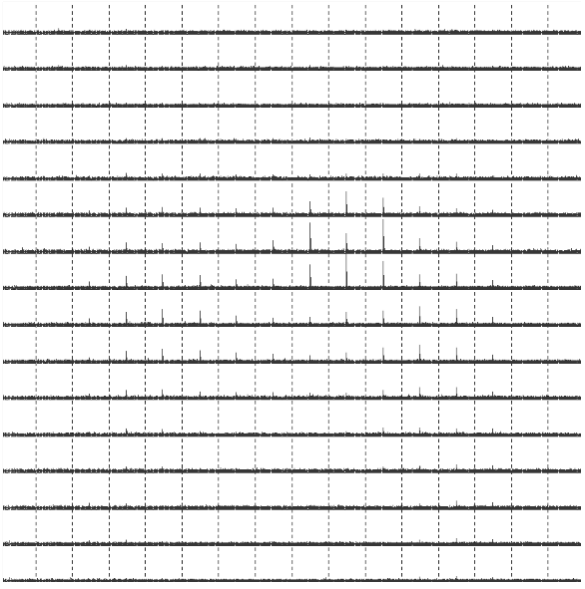

Figure S5.2 ^{19}F CSI matrix a piece of beef liver following injection of a 4 mM PBS solution of **Ru(III)(ImCF$_3$)$_2$**. The tumour was then placed back in the same solution in a test-tube. The ^{19}F CSI parameters were as described in section S2.4 with TR 300 ms.

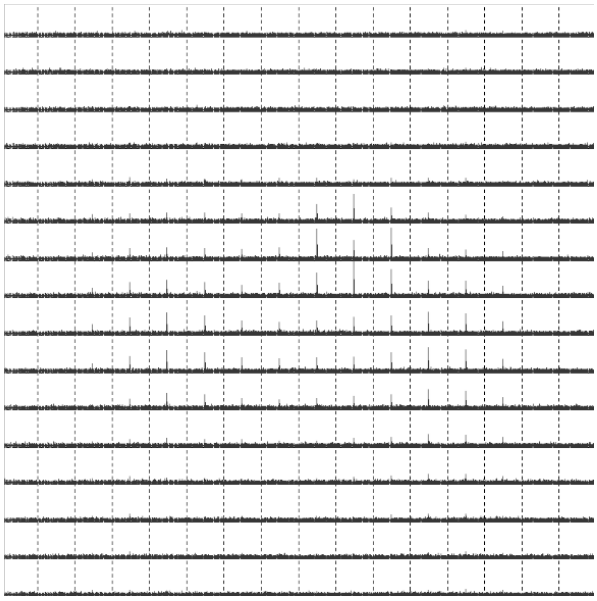

Figure S5.3 ^{19}F CSI matrix of a piece of beef liver following injection of a 4 mM PBS solution of **Ru(III)(ImCF$_3$)$_2$**. The tumour was then placed back in the same solution in a test-tube. The ^{19}F CSI parameters were as described in section S2.4 with TR 1000 ms.

S5.2 ^{19}F CSI Matrices of an MBA-MB-231 Human Breast Adenocarcinoma Tumour

a) **Ru(III)(ImCF$_3$)$_2$** b) **Ru(II)(ImCF$_3$)$_2$**

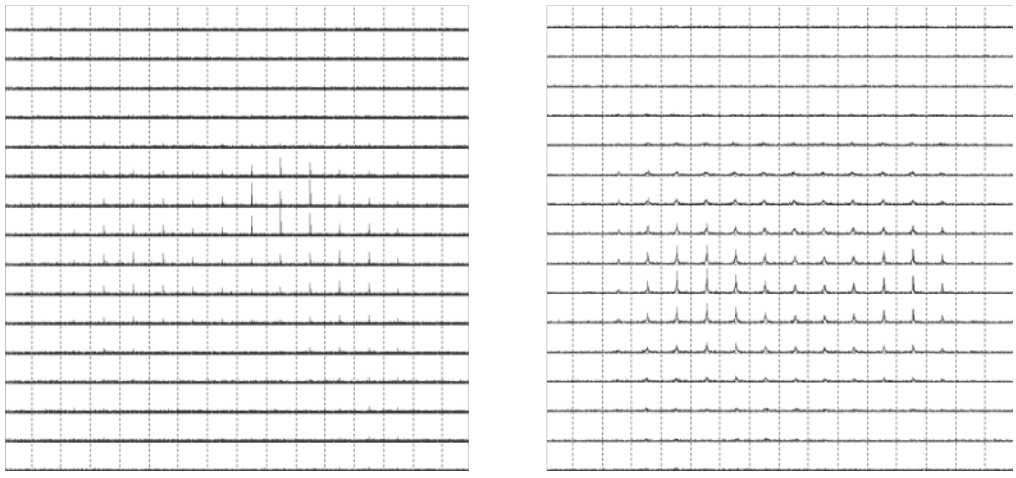

Figure S5.4 ^{19}F CSI matrix of an MBA-MB-231 human breast adenocarcinoma tumour following an injection of a 4 mM PBS solution of a) **Ru(III)(ImCF$_3$)$_2$** and b) **Ru(II)(ImCF$_3$)$_2$**. Following the injection, the tumour was placed in a test tube containing the same solution for imaging.

S5.3 Timepoints of ^{19}F CSI Voxels from Tumour Tissue Experiments

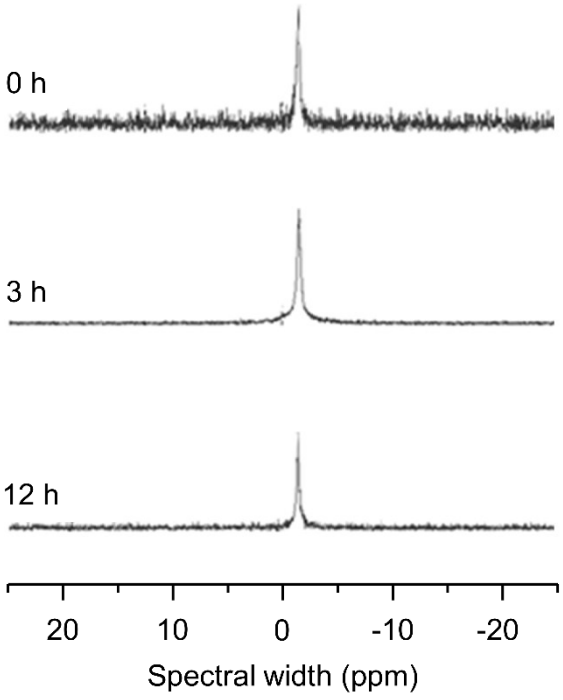

Figure S5.5 Individual ^{19}F CSI spectra from surrounding solution of MBA-MB-231 human breast adenocarcinoma tumour tissue at 0, 3, and 12 h following injection of a 4 mM solution of **Ru(III)(ImCF$_3$)$_2$**.

References

1 S. W. Chang, A. R. Lewis, K. E. Prosser, J. R. Thompson, M. Gladkikh, M. B. Bally, J. J. Warren and C. J. Walsby, *Inorg. Chem.*, 2016, **55**, 4850-4863.

2 D. W. McRobbie, E. A. Moore, M. J. Graves and M. R. Prince, in *MRI from Picture to Proton*, Cambridge University Press, Cambridge, 2nd edn., 2006, pp. 79-107.

3 J. Hennig, A. Nauerth and H. Friedburg, *Magn. Reson. Med.*, 1986, **3**, 823-833.

4 A. Sodickson, in *Handbook of Neuro-Oncology Neuroimaging*, eds. H. B. Newton and F. Jolesz, Academic Press, San Diego, 1st edn., 2008, ch. 18 pp. 128-135.

5 M. Schär, B. Strasser and U. Dydak, in *eMagRes*, eds. R. K. Harris and R. L. Wasylishen, John Wiley & Sons, Ltd, 2016, vol. 5, pp. 1291-1306.

6 L. Starke, T. Niendorf and S. Waiczies, in *Methods Mol. Biol.* , Springer, New York, NY, 2021, vol. 2216, pp. 711-722.

7 R. M. Henkelman, *Med Phys*, 1985, **12**, 232-233.

8 NEMA Standards Publication, MS 9-2008 (R2014), Characterization of Phased Array Coils for Diagnostic Magnetic Resonance Images, 2008